J Mater Sci (2010) 45:5704–5710
DOI 10.1007/s10853-010-4640-z

# Photoluminescence and photoreactivity affected by oxygen defects in crystal-oriented rutile thin film fabricated by molecular precursor method

**Hiroki Nagai · Sohei Aoyama · Hiroki Hara · Chihiro Mochizuki · Ichiro Takano · Tohru Honda · Mitsunobu Sato**

Received: 22 December 2009 / Accepted: 21 May 2010 / Published online: 5 June 2010


**Abstract** This article describes the post-annealing treatment of a rutile thin film, which was fabricated on a quartz glass substrate by heat treating a precursor film in air for 15–60 min by using a process involving a Ti complex of EDTA. The transparent, crack-free rutile thin films thus obtained were characterized by means of X-ray diffraction, X-ray photoelectron spectroscopy, and field emission scanning electron microscopy. The photoluminescence emission band of the post-annealed rutile thin films appeared at ca. 800 nm, which is in the extraordinary low-energy region, although no emission band in the region could be observed for the rutile thin film before annealing. It was revealed that the extraordinary emission band of the thin films at 800 nm is strongly related both to the orientation of the constituent crystals along the (110) plane and to the incorporation of O atoms into the O-defect sites that were in the rutile thin film before the post-annealing treatment.

H. Nagai · S. Aoyama · H. Hara · C. Mochizuki · M. Sato (✉)
Coordination Engineering Laboratory, Faculty of Engineering, Kogakuin University, 2665-1 Nakano, Hachioji City, Tokyo 192-0015, Japan
e-mail: ft10302@ns.kogakuin.ac.jp

I. Takano
Department of Electrical Engineering, Faculty of Engineering, Kogakuin University, 2665-1 Nakano, Hachioji City, Tokyo 192-0015, Japan

T. Honda
Department of Electronic Engineering, Faculty of Engineering, Kogakuin University, 2665-1 Nakano, Hachioji City, Tokyo 192-0015, Japan

## Introduction

Titania is the most extensively used in fields, such as solar energy conversion and photoluminescence (PL), due to its exceptional optical and electronic properties, non-toxicity, low cost, and long-term stability [1–5].

The molecular precursor method, which we recently developed as a novel wet process for the thin film fabrication of metal oxides and calcium phosphates, is based on the film formation of alkylammonium salts of stable metal complexes whose ligands are aminopolycarboxylic acids such as ethylenediamine-N, N, N′, N′-tetraacetic acid (EDTA = $H_4$edta) [6–10]. This method solves several problems that arise because of the necessity of polymerization in the conventional sol–gel procedure. Heat treating the precursor films that adhere to substrates, which is also carried out in the conventional sol–gel method, is useful for obtaining transparent and crack-free thin films of various metal oxides and phosphates. The solutions employed in the molecular precursor method have better stability, water resistance, and miscibility than those employed in the sol–gel method.

We recently found that a visible light-responsive rutile thin film having high photoreactivity under UV irradiation can be formed by the molecular precursor method [10]. Several O-defect sites in the rutile lattice could be formed by heat treating the precursor films in an Ar gas flow; the Ti–N bonds of the molecular precursor complex were involved in the process of defect site formation. Effective electron trapping by the O-defect sites in rutile thin films suppresses the process of recombination between the photoinduced electron–hole pairs, thereby giving rise to the abovementioned high photoreactivity in these films.

PL emission has been widely used to investigate the efficiency of charge carrier trapping, migration, and transfer,

and to understand the fate of electron–hole pairs in semiconductor particles. It is, therefore, important to examine the PL emission of semiconductor particles because the position and intensity of the PL band is directly related to the photoreactivity of the particles [11]. In this study, we report on the PL and photoreactive properties of a rutile thin film, both before and after annealing, when it is fabricated by the molecular precursor method. The relationship between the O deficiency and the PL emission was examined to understand the unprecedentedly high photoreactivity of the rutile thin film. Furthermore, the level of crystal orientation of the rutile thin film was quantitatively evaluated on the basis of data from X-ray diffraction (XRD) analyses, and the amount of oxygen supplied during the annealing process was analyzed by X-ray photoelectron spectroscopy (XPS) measurements. The growth of crystals and particles was also investigated by crystallite-size measurements and field emission scanning electron microscopy (FE-SEM) observations.

## Experimental

### Materials

Ethylenediamine-N, N, N′, N′-tetraacetic acid (EDTA) and titanium tetraisopropoxide ($Ti(O^iPr)_4$) were purchased from Kanto Chemical Co., Inc. Dibutylamine and 30% $H_2O_2$ were purchased from Wako Pure Chemical Industries, Ltd., and from Santoku Chemical Industries Co., Ltd., respectively. Ethanol was purchased from Ueno Chemical Industries, Ltd. Methanol was purchased from Taisei Chemical Co., Ltd. These solvents were dried on 4A molecular sieves prior to use. Other materials were used without further purification. Polished quartz glass was purchased from Akishima Glass Co., Ltd. The glass substrate to be coated (dimensions: 20 × 20 × 1.1 $mm^3$) was washed in 2-propanol for 15 min with sonicated stirring and then dried in a drying oven at 70 °C.

### Preparation of coating solution $\mathbf{S_{MP}}$ and fabrication of rutile thin film **R**

The precursor solution $\mathbf{S_{MP}}$ containing a $Ti^{4+}$ complex of EDTA was prepared and rutile thin film **R** was fabricated using the solution in accordance with the method reported in previous studies of Nagai and co-workers [8–10].

### Post-annealing treatment of the **R** thin film

The post-annealing treatment of the fabricated **R** thin film was carried out in air at 700 °C for 15, 30, and 60 min. The number in the notation of the post-annealed films indicates the annealing time (min); for example, **R-PA15** indicates that post-annealing treatment of the **R** thin film was carried out for 15 min.

### Structural characterization of thin films

X-ray diffraction (XRD) measurements of the titania thin films were carried out on an MXP-18AHF22 X-ray diffractometer (Bruker AXS) using the $\theta$–$2\theta$ scan method; graphite monochromatized Cu-$K\alpha$ radiation was employed at a voltage and currents of 45 kV and 300 mA, respectively. The extent orientation could be estimated from the XRD peak intensity by using the Lotgering method [12]. The terms $I(hkl)_{ideal}$ and $\Sigma I(hkl)_{ideal}$ are defined as the intensity of the peak attributable to the specific plane ($hkl$) and the sum of each intensity obtained for the non-oriented rutile crystals, respectively; thus, $P_0$ can then be expressed as

$$P_0 = I(hkl)_{ideal}/\Sigma I(hkl)_{ideal} \quad (1)$$

In this study, each $I(hkl)_{ideal}$ value was cited from the standard data of the corresponding rutile phase [13].

The definitions of the terms $I(hkl)_{obsd}$ and $\Sigma I(hkl)_{obsd}$ for the thin films **R** and **R-PA***n* are identical to those for $\Sigma I(hkl)_{ideal}$ and $I(hkl)_{ideal}$ in Eq. 1, respectively, and the $P_n$ value can be calculated as

$$P_n = I(hkl)_{obsd}/\Sigma I(hkl)_{obsd} \quad (2)$$

The Lotgering orientation factor $f$ is defined as

$$f = (P_n - P_0)/(1 - P_0) \quad (3)$$

The factor $f$ is defined for $P$ or $P_0$ values over a certain range of $2\theta$. As the level of orientation increases, the $f$ value will increase from 0 to 1. The factor $f$ is, therefore, a measure of the crystal phase orientation.

The crystallite size of the rutile crystals was measured using the typical Scherrer-Hall method; for this purpose, parallel beam optics were used with the identical instrument mentioned above.

### Chemical identification of the thin films

The XPS measurements were obtained to characterize the thin films. A Phi Quantum 2000 scanning electron spectroscopy for chemical analysis (ESCA) microprobe equipped with a focused monochromatic Al-$K\alpha$ X-ray source (1486.6 eV) was employed to evaluate the states and amounts of the elements Ti, O, N, C, and Si in thin films. Chemical shift data were charge referenced to the center of the C–C/C–H peak at 284.6 eV. The resolution for each measurement was 0.2 eV.

Depth profiles in the $Ar^+$ etching mode were obtained by the same instrument after $Ar^+$ ion beam bombardment

was carried out at 2 kV and 18 μA $cm^{-2}$ for 3 min to remove surface oxides. Each 15-layer segment was etched stepwise every 3 min on being bombarded with $Ar^+$ ions at the same accelerating energy of 2.0 kV, and measurements for the thin films were performed over an area of 50 $\mu m^2$. In order to investigate the O/Ti ratios of the thin film surfaces, XPS spectra of Ti 2p and O 1s peaks were also recorded without $Ar^+$ ion beam bombardment.

### PL measurement of the thin films

Room temperature PL spectra of the thin films on the quartz glass substrate were obtained over a wavelength range of 190–850 nm by a USB-2000 miniature fiber optic spectroscope (Ocean Optics). The measurements were performed using the 325-nm He-Cd laser line (Kimmon Electric IK 3351R-G) as an excitation source with an emitting power of 1.0 mW.

### Photoreactivity measurements of the thin films

The photoreactivity of each film occupying an area of 20 × 20 $mm^2$ on the substrate was measured in terms of the decoloration rate of a dye, methylene blue (MB), in a 10-mL aqueous solution (0.01 mmol $L^{-1}$) at 20 (±1) °C. Black light (FL10BL-B, National) was used for UV light irradiation. The distances of the black-light sources from the sample surfaces were adjusted to maintain a UV light intensity of 1.2 mW $cm^{-2}$ at 365 nm; the intensity was measured by an ultraviolet meter (UVR-400, Iuchi). Fluorescent light (True Light, Duro Test) was also incident on samples; subsequent to the removal of light with wavelengths shorter than 400 nm by means of a cut-off filter, the intensity of the visible light incident on the samples was 0.8 mW $cm^{-2}$; the intensity was measured by an illuminometer (LX-105, Custom). The decoloration rate $v$ was estimated by the decrease in the absorption value of each test solution at 664 nm in accordance with the method described in our previous reports [8–10].

## Results

### Structure of the thin films

The XRD patterns of the post-annealed thin films **R-PA***n* ($n$ = 15, 30, and 60 min), along with that of the thin film **R**, are shown in Fig. 1. The peaks at $2\theta$ = 27.4°, 36.1°, and 54.3° observed in each XRD pattern can be attributed to the (110), (101), and (211) planes of the rutile crystals [13].

Table 1 lists the calculated results obtained for the extent orientation factor $f$ as well as the mean crystallite size of the rutile crystals in each film.

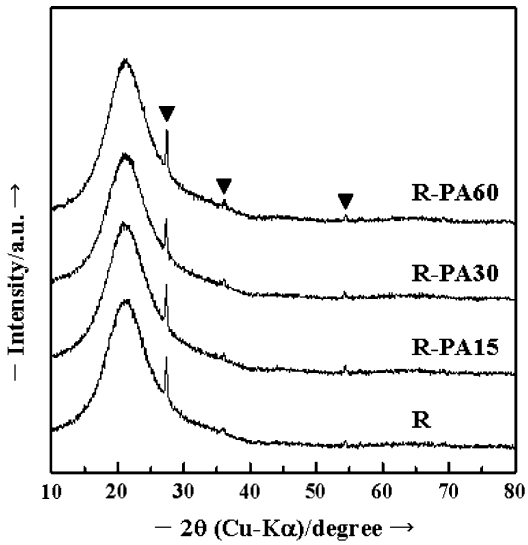


**Fig. 1** XRD patterns of the thin film **R**, and those of **R-PA***n* ($n$ = 15, 30, and 60). The thin film **R** was fabricated by heat treating the precursor film at 700 °C in an Ar gas flow, and the thin films **R-PA***n* were obtained by post annealing the thin film **R** at 700 °C in an air atmosphere for 15, 30, and 60 min. The peaks assignable to the rutile phase are shown by the indicator *filled down-pointing triangle*

Figure 2 shows the surface appearance of the following four thin films: (A) **R**, (B) **R-PA15**, (C) **R-PA30**, and (D) **R-PA60**. The surface roughness of each film was ca. 10 nm, which is equal to the resolution of the stylus profilometer used in this study. The mean size of the grains in the **R**, **R-PA15**, **R-PA30**, and **R-PA60** thin films was ca. 90, 100, 110, and 130 nm, respectively.

### Chemical identification of the thin films by XPS

The depth profiles measured by XPS are shown in Fig. 3. Small amounts of C and N atoms in the range 0.34–2.42 at.% and 0.08–0.28 at.%, respectively, were detected in the thin film **R**. Furthermore, as shown in the figure, the quantities of C and N atoms in the thin film **R** decreased with an increase in the time for annealing treatment in air.

Table 1 lists the O/Ti ratio on the thin film surface (the first layer) and the average O/Ti ratios of the next nine deepest layers, as obtained from the depth profile of each thin film.

### PL spectra of the thin films

The PL emission spectra of all the samples measured in the wavelength range from 190 to 850 nm are shown in Fig. 4. The emission band at 800 nm was observed in the spectra of the post-annealed thin films **R-PA***n*, although no emission band was observed in the PL spectrum of the **R** thin film at the same range.

**Table 1** The crystallite sizes, orientation factors, and O/Ti ratios of rutile crystals in the **R** thin film and in the post-annealed **R-PAn** thin films

| Film | Crystallite size[a]/nm | Orientation factor; *f* | O/Ti ratios | |
|---|---|---|---|---|
| | | | Surface | Deeper portion |
| **R** | 15(2) | 0.35 | 1.74 | 1.75 |
| **R-PA15** | 21(3) | 0.67 | 1.84 | 1.73 |
| **R-PA30** | 21(3) | 0.69 | 1.89 | 1.79 |
| **R-PA60** | 20(4) | 0.75 | 1.94 | 1.85 |

The crystallite size of rutile was measured with a typical Scherrer-Hall method employing the peaks assignable to (110), (101), and (211) of rutile

The extent of the orientation was estimated in terms of Logtering orientation factor, *f*, from the XRD peak intensities (*I*). For calculating the orientation factor, the intensity data of non-oriented rutile was cited from the JCPDS card 21-1276

The O/Ti ratios determined by the XPS peak areas of O 1s and Ti $2p_{3/2}$ peaks observed from the surfaces of **R** and post-annealed thin films. The XPS peaks of the thin film surface were measured without bombarding $Ar^+$ ion beam. The peak areas of O 1s and Ti 2p were calculated by FWHM, and peak heights measured at the positions 531.0 and 459.0 eV, respectively

The averaged O/Ti ratios determined by the XPS peak areas of O 1s and Ti $2p_{3/2}$ peaks of **R**, and post-annealed thin films. The XPS peaks of thin films were measured after bombarding $Ar^+$ ion beam with 2 kV and 18 μA $cm^{-2}$ for 3 min, to remove surface oxides. The peak areas of O 1s and Ti 2p were calculated by FWHM and peak heights measured at the positions 531.0 and 459.0 eV, respectively, obtained from each depth profile in $Ar^+$ ion etching mode

[a] The estimated standard deviations are presented in parentheses

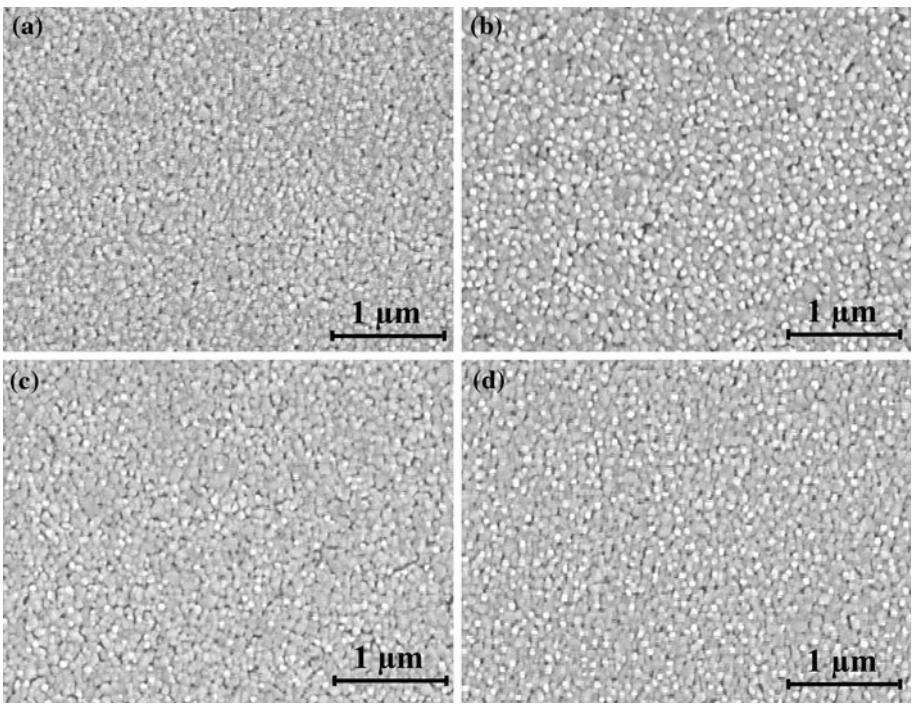


**Fig. 2** Surface appearances of the four thin films, **a R**, **b R-PA15**, **c R-PA30**, and **d R-PA60**, whose thickness is 100 nm on a quartz substrate observed using an FE-SEM

### Photoreactivity of thin films

The photoreactivities of the thin films under UV and visible light irradiation are summarized in Table 2; the photoreactivities measured under dark conditions are also provided as reference values, indicating the effects of adsorption on the samples and vessels and the self-decoloration of MB at the 20 (±1) °C. The *v* values that are larger than those obtained under dark conditions can be used to determine the degree of photoreaction induced by light irradiation on the films.

## Discussion

### Orientation and growth of rutile crystals in thin films

The extent orientation factor *f* for the (110) plane of the **R-PA***n* thin films increased with the annealing time in air (Table 1). Consequently, the *f* value of the **R** thin film was the smallest among the investigated thin films. However, the *f* value of the **R** thin film was larger than the values reported in the literature for processes in which rutile thin films were fabricated by the sol–gel method on several

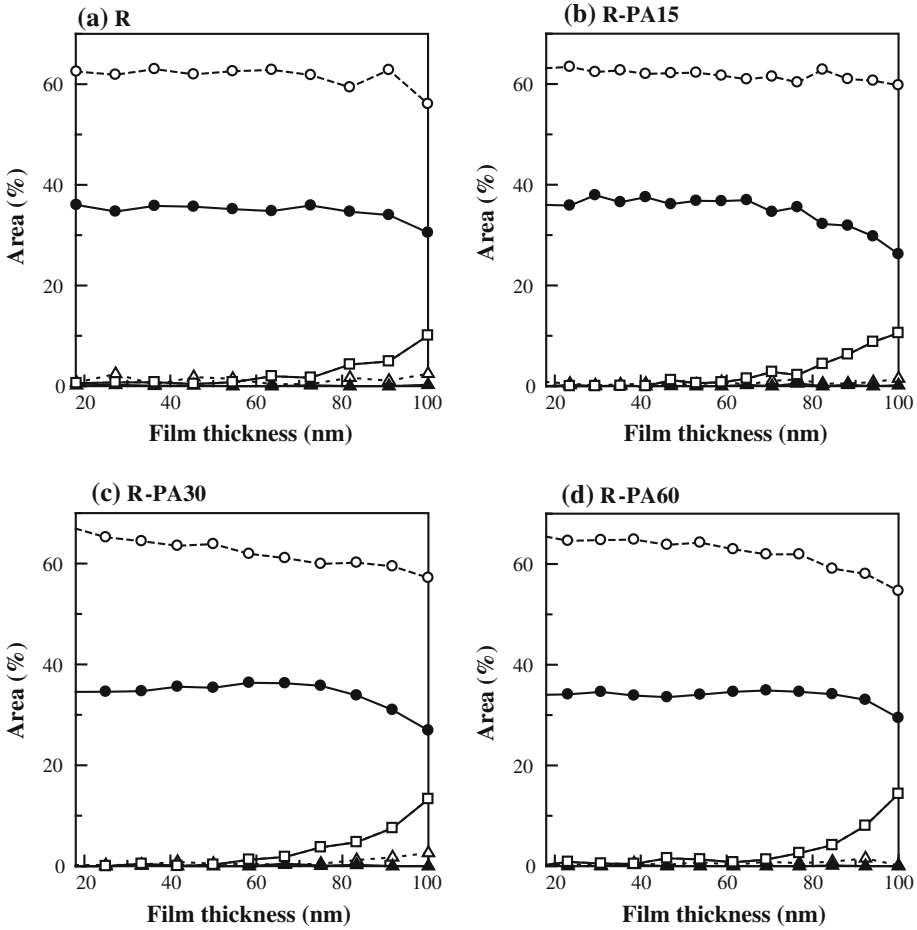


**Fig. 3** Depth profile of the elements, Ti, O, N, C, and Si in the thin films (A) **R**, (B) **R-PA15**, (C) **R-PA30**, and (D) **R-PA60**. The energy levels of the five atoms are indicated in parentheses, *filled circle* (Ti 2p), *open circle* (O 1s), *filled triangle* (N 1s), *open triangle* (C 1s), *open square* (Si 2p). Measurements of each of the 15 layers etched stepwise for every 3 min by bombarding $Ar^+$ ion with 2 kV and 18 μA $cm^{-2}$ were performed at an area of 50 $\mu m^2$ of the thin films

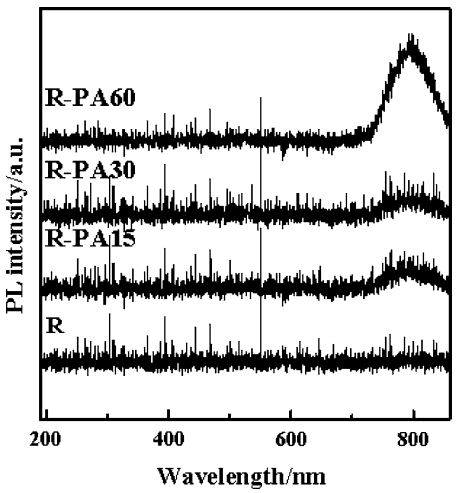


**Fig. 4** The photoluminescence emission spectra of the thin films, **R** and **R-PA***n* ($n = 15$, 30, 60). The spectra were examined in the wavelength range of 190–850 nm at room temperature

**Table 2** The $v$ [nmol $L^{-1}$ $min^{-1}$] of decoloration rate of 0.01 mol $L^{-1}$ MB solution by the photoreaction with each thin film under UV or vis light irradiation

| Film | $v^a$/nmol $L^{-1}$ $min^{-1}$ | | |
|---|---|---|---|
| | UV | vis | Dark |
| **R** | 25(1) | 17(1) | 3(1) |
| **R-PA15** | 20(1) | 15(1) | 3(1) |
| **R-PA30** | 21(1) | 16(1) | 3(1) |
| **R-PA60** | 20(1) | 15(1) | 3(1) |

A black light was used for UV-light irradiation. The distances of the black-light sources from the sample surfaces were adjusted to maintain the UV-light intensity of 1.2 mW $cm^{-2}$ at 365 nm. The intensity of the visible light on the samples was 0.8 mW $cm^{-2}$ with the fluorescent light, after removing the light with wavelengths shorter than 400 nm using a cut-off filter. The decoloration rate was measured by the decrease of absorption value at 664 nm of each test solution. Those obtained from the data measured under dark are also indicated

[a] The estimated standard deviations are presented in parentheses

substrates such as quartz glass, alumina, and single crystals of quartz or silicon [14]. This result may be related to the different mechanisms governing the formation of the rutile lattice. In the case of the sol–gel method, the $Ti^{4+}$ and $O^{2-}$ ions that are tightly linked in titanoxane polymers formed by the condensation of partially hydrolyzed alkoxide might be rearranged to form the rutile lattice at a higher temperature. On the other hand, in the case of molecular

precursor method, the small units composed of $Ti^{4+}$ and $O^{2-}$ ions with higher mobility could be formed when the organics were decomposed and removed by heat treating the precursor complex. Therefore, a rutile thin film with a higher level of crystal orientation could be formed at the low temperature employed in this present study.

When the annealing treatment was carried out for 15 min, the crystallite size of the **R** thin film increased, while that of the **R-PA*n*** thin films remained almost constant (Table 1). These results indicate that crystallite growth at a temperature of 700 °C was completed by heat treatment over a period of 30–45 min. The additional thermal energy was consumed mainly for the process of grain growth after the crystallite growth, because the grain size gradually increased with the annealing time.

The crystal-oriented films of rutile were mainly fabricated by several methods using physical vapor deposition (PVD) in vacuum chambers, as well as chemical vapor deposition (CVD) [15–17]. Through a wet process, crystal-oriented thin films of anatase were fabricated employing an aqueous $TiCl_3$ solution, in the case of a hydrothermal procedure with the application of a magnetic field [18]. The procedures adopted in this study for heat treating precursor films containing a titanium complex in an Ar gas flow and sequential annealed treatment in air are extremely simple. Because both high crystallinity and a high level of crystal orientation are generally important for realizing thin film-based devices with high performance, it is important for the molecular precursor method to be able to fabricate rutile thin films that are highly crystallized and oriented along the (110) plane on glass substrates.

The extent crystal orientation was evaluated on the basis of the XRD peak intensities. Therefore, the estimated $f$ value of the thin film **R** might be relatively smaller than the net value obtained from the atomic arrangement of the rutile lattice, because the peak intensity of the (110) plane strongly depends on the amount of oxygen defects in the lattice. With an increase in the annealing time, a simultaneous increase in the O/Ti ratio and extent orientation factor $f$ was observed. Consequently, it can be deduced that the atomic arrangement of the rutile lattice originally showed an extremely high level of crystal orientation and did not gradually develop as a result of the annealing treatment.

### PL spectra of the R and R-PAn thin films

The peak position of the PL emission band obtained for rutile crystals is usually observed at ca. 450 nm [19]. The PL emission bands of all the **R** and **R-PA*n*** thin films in this study, however, could not be detected at ca. 450 nm (Fig. 4).

Nakamura et al. reported that in the case of a rutile single crystal, the PL emission band attributable to the (110) plane can be observed at 810 nm [20]. Taking into account the high levels of crystal orientation with reference to the (110) plane in the **R** and **R-PA*n*** thin films, the PL emission bands observed in the spectra of the **R-PA*n*** thin films can be attributed to the rutile crystals oriented along the (110) plane in these thin films.

### Oxygen in rutile lattice as the recombination center of photoinduced electron–hole pairs

In the case of the O-deficient rutile thin film **R** with high photoreactivity, PL emission was not observed in the range of 190–850 nm. Thus, as proposed previously, the O-defect sites on the rutile thin film may suppress the recombination of the photoinduced electron–hole pairs by electron trapping. In contrast, the PL emission from rutile thin films after post-annealing treatment in air may be due to the oxide ions that are supplied to the O-defect sites, mainly on the film surface, because they can function as recombination centers. As a result, it can be deduced that the lattice oxygen of titania, especially in rutile thin films, functions as a recombination center for the photoinduced electron–hole pairs.

It is known that the reduction of rutile surfaces by heated hydrogen activates the photoreactivity of these surfaces [21]. The formation of an oxygen deficiency by the removal of oxygen atoms causes the usually inactive rutile surface to become chemically active. This study revealed that the generally high photoreactivity of the **R** thin film can be suppressed when oxygen is supplied during the annealing process. It is important for the high level of photoreactivity in these films to be maintained following oxygen supply to the surface by the post-annealing treatment (Table 2), although the O/Ti ratios of the **R** thin film surfaces were smaller than those of the post-annealed thin films. These results indicate that the enhanced photoreactivity is related not only to the surface but also to the inner part of the thin films on account of the inter-particle electron transfer (IPET) effect, as was proposed in our previous article [10].

## Conclusion

The changes in both the orientation factor $f$ and the PL emission behaviors of rutile thin films comprising crystals oriented along the (110) plane and containing O-defect sites can be attributed to the gradual supply of oxygen atoms to the defect sites existing in these thin films. The details of these changes are as follows:

(1) Heat treatment of the precursor film containing a titanium complex leads to the formation of an **R** thin film comprising rutile crystals oriented along the (110) plane

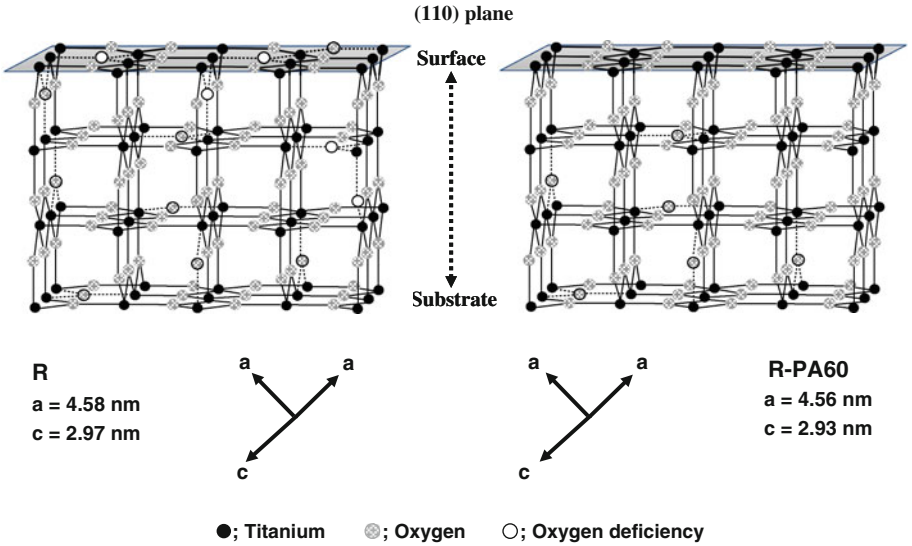


**Plate 1** Proposed schematic for the (110) plane-orientated O-deficient **R** (*left*) and **R-PA60** (*right*) thin films are shown. Cell parameters were refined by a least square method

and containing a large amount of oxygen defects (Plate 1-left). (2) Atmospheric oxygen is gradually supplied mainly to the surface of the thin films with crystals oriented along the (110) plane, as has been indicated by the XPS spectra (Fig. 3). (3) The extent orientation factor *f* increased with an increase in the (110) plane with higher electron density due to the supplied oxygen atoms. (4) The preferential supply of oxygen to the (110) plane of the rutile surface (Plate 1-right) explains both (A) the appearance of the PL emission band when the investigated rutile thin film is annealed in air and (B) the dependence of the emission intensity on the annealing time of the **R-PA***n* thin films.

It is generally difficult to fabricate titania thin films comprising oriented crystals by chemical methods without using some form of physical control such as magnetic fields. In contrast, this study confirmed that rutile thin films comprising crystals oriented along the (110) plane can be easily formed on a quartz glass substrate using the molecular precursor method. The emission position and intensity of the PL emission band are strongly dependent on the atomic-level structures of the surfaces, although the photoreactivity of the investigated films did not seem to be significantly affected. Thus, in these films, the driving forces that lead to self-assembled crystal orientation are of great interest.

## References


1. Fujishima A, Rao TN, Tryk DA (2000) J Photochem Photobiol C 1:1
2. O'Regan B, Grätzel M (1991) Nature 353:737
3. Nemoto J, Horikawa M, Ohtani K, Shibata T, Ueno H, Hoshino M, Kaneko M (2007) J Appl Electrochem 37:1039
4. Bard AJ (1980) Science 207:139
5. Ni M, Leung MKH, Leung DYC, Sumathy K (2007) Renew Sustain Energy Rev 11:401
6. Nishide T, Sato M, Hara H (2000) J Mater Sci 35:465. doi: 10.1023/A:1004731804075
7. Sato M, Hara H, Nishide T, Kuritani H, Sawada Y (1996) J Mater Chem 6:1767
8. Nagai H, Mochizuki C, Hara H, Takano I, Sato M (2008) Sol Energy Mater Solar Cells 92:1136
9. Nagai H, Hasegawa M, Hara H, Mochizuki C, Takano I, Sato M (2008) J Mater Sci 43:6902. doi:10.1007/s10853-008-2993-3
10. Nagai H, Aoyama S, Hara H, Mochizuki C, Takano I, Baba N, Sato M (2009) J Mater Sci 44:861. doi:10.1007/s10853-008-3185-x
11. Jung KY, Park SB (1999) J Photochem Photobiol A 127:117
12. Lotgering FK (1959) J Inorg Nucl Chem 9:113
13. JCPDS Card 21-1276
14. Nikilić LM, Radonjić L, Srdić VV (2005) Ceram Int 31:261
15. Hosono E, Fujihara S, Kakiuchi K, Imai H (2004) J Am Chem Soc 126:7790
16. Sasaki T, Ebina Y, Tanaka T, Harada M, Watanabe M (2001) Chem Mater 13:4661
17. Miyauchi M, Tokudome H (2007) Appl Phys Lett 91:043111
18. Uchikoshi T, Suzuki T, Imura S, Tang F, Sakka Y (2006) J Eur Ceram Soc 26:559
19. Tamashita H, Ichihashi Y, Zhang SG, Matumura Y, Souma Y, Tatsumi T, Anpo M (1997) Appl Surf Sci 121/122:305
20. Nakamura R, Okamura T, Ohashi N, Imanishi A, Nakato Y (2005) J Am Chem Soc 127:12975
21. Fujishima A, Honda K (1972) Nature 238:37